NASA SP-330

APOLLO 17

Preliminary Science Report

PREPARED BY

LYNDON B. JOHNSON SPACE CENTER

Scientific and Technical Information Office 1973

NATIONAL AERONAUTICS AND SPACE ADMINISTRATION

Washington, D.C.

9. Heat Flow Experiment

Marcus G. Langseth, Jr.,[a†] *Stephen J. Keihm,*[a] *John L. Chute, Jr.*[b]

The objectives of the heat flow experiment (HFE) were to make a direct measurement of the vertical component of heat flow from the lunar interior through the surface and to determine the thermal properties of the upper 3 m of the lunar regolith.

The age of the Moon is placed at 4.6×10^9 yr. For a planetary body as small as the Moon, much of the initial heat energy has been lost to space since formation. Even if the Moon were initially at molten temperatures, the present flux at the surface would be small. The major contribution to the surface heat flow comes from heat generated by the disintegration of long-lived radioisotopes of uranium (^{235}U and ^{238}U), potassium (^{40}K), and thorium (^{232}Th). Thus, the present surface heat flux reflects the abundance of these isotopes to a depth of approximately 300 km, or 43 percent of the volume of the Moon. It is now certain that extensive differentiation occurred during the early history of the Moon that would concentrate these isotopes in the outer shells. In this case, the present surface heat flow would very nearly indicate the total abundance of these isotopes.

More than 5000 heat flow determinations made on Earth show the average global flux to be 6.3×10^{-6} W/cm^2 (ref. 9-1). (Throughout this report, W-sec will be used as the unit of heat energy. Other commonly used units are the calorie, which equals 4.18 W-sec, and the erg, which equals 10^{-7} W-sec. The average Earth heat flow is 1.5×10^{-6} cal/cm^2-sec and 63 ergs/cm^2-sec.) Urey (ref. 9-2) pointed out that the total rate of heat flow from the Earth is essentially equal to the total rate of heat production in the Earth if it were constituted of materials with chondritic abundances of uranium, potassium, and thorium. However, Gast (ref. 9-3) showed that Earth rocks were strongly depleted in potassium relative to solar and chondritic abundances, which led Wasserburg et al. (ref. 9-4) to propose that, to explain the heat flow from Earth, a higher abundance of uranium (nearly 3 times that of chondrites) is needed. They estimated a uranium abundance of approximately 30 ppb for the Earth.

The large variations of heat flow observed over the surface of the Earth are principally related to the present tectonism of the Earth lithosphere (ref. 9-5). The largest variations are observed at extensional and compressional boundaries of vast lithospheric plates that are moving relative to each other. Seismic observations (ref. 9-6) and the preservation of ancient surface features on the Moon demonstrate that no comparable tectonic movements have occurred on the Moon for the past 3×10^9 yr. The Moon is tectonically dead compared to the Earth; therefore, any variations in surface heat flow over the surface should reflect either deep-seated changes in abundances of radioisotopes or in convective patterns in the Moon. Because of the static nature of the outer crust of the Moon, heat flow determinations at a single location might be quite representative of a very large region of the Moon if local surficial effects such as refraction by conductive inhomogeneities and topography are properly accounted for.

Numerous attempts have been made to determine the surface heat flow from the Moon by detecting thermal radiation from the Moon in the microwave band. Because of the partial transparency of lunar surface material, energy with wavelengths greater than 1 mm received at Earth-based antennas originates in the subsurface and contains information on subsurface temperatures. By making estimates of thermal and electrical properties, the heat flow can be determined from the change of brightness temperature with wavelength. The earliest heat flow determination was that of Baldwin (ref. 9-7), who estimated an upper limit of 1×10^{-6} W/cm^2. Russian investigators estimated the heat flow to be very

[a]Lamont-Doherty Geological Observatory.
[b]H. H. Lehman College, City University of New York.
[†]Principal Investigator.

nearly equal to that of the Earth, based on a very careful set of radio-telescope observations in the wavelength band 3 to 50 cm (ref. 9-8). These same measurements were later revised by using different thermal properties and a layered model to give heat flows in the range 3×10^{-6} to 4×10^{-6} W/cm^2 (ref. 9-9).

During the Apollo 15 mission, the first direct measurement of heat flow through the lunar surface was made at Rima Hadley (lat. 26°06′ N and long. 3°39′ E). A second measurement was made during the Apollo 17 mission at the Taurus-Littrow site (lat. 20°10′ N and long. 30°46′ E). At Taurus-Littrow, two probes to determine heat flow were emplanted approximately 11 m apart. Analysis of data taken during the first 45 days after emplacement indicates that the heat flow is 2.8×10^{-6} W/cm^2 (0.67 μcal/cm^2-sec) at one probe location and 2.5×10^{-6} W/cm^2 (0.60 μcal/cm^2-sec) at the second probe location. For comparison, the value measured at Rima Hadley is 3.1×10^{-6} W/cm^2 (0.74 μcal/cm^2-sec). The Rima Hadley measurement and Taurus-Littrow probe 1 measurement have an estimated error of ± 20 percent. The probe 2 measurement at Taurus-Littrow has a slightly larger uncertainty because the heat flow appears to be locally disturbed. These measurements have not been corrected for local topography.

EXPERIMENT DESCRIPTION

Experiment Concept and Design

The concept on which the HFE is based is the direct measurement of the vertical flow of heat through the regolith. The measurement should be made far enough below the surface so that the time-varying heat flow resulting from the very large diurnal variations of surface temperature is small compared with the flow from the interior. At Taurus-Littrow, this depth is approximately 100 cm. Below this depth, the increase in temperature with depth results principally from the hotter lunar interior. The outward flow of heat is directly proportional to the rate of temperature increase with depth. These quantities are related by the equation

$$F_z = -k_m(dT/dz) \qquad (9\text{-}1)$$

where F_z is the vertical component of the heat flow, T is the temperature, z is the depth, and the constant k_m is the thermal conductivity. The negative sign indicates that the heat flows in a direction opposite to the increase of temperature.

The experiment is designed to measure accurately the vertical temperature gradient in the lunar soil to a depth of 2.3 m. Surface temperature measurements are also made that can be used to deduce the thermal properties of the upper 10 to 15 cm of regolith. In situ measurements of thermal conductivity of the regolith at depths where the gradient is measured are also performed. Two measurements of heat flow at locations separated by approximately 10 m are made to detect possible lateral variations.

The essential parts of the heat flow instrument are two identical temperature-sensing probes. Each probe consists of two 50-cm-long sections (fig. 9-1(a)). In each probe section are two platinum resistance bridges; each bridge consists of four 500-ohm filamentary platinum elements interconnected by Evanohm wire (fig. 9-1(b)). Opposing arms of a bridge are wound together in a single sensor housing; two sensor housings, comprising a complete bridge, are mounted at opposite ends of a probe section.

Voltage measurements on a bridge can be interpreted by accurate calibrations in terms of average bridge temperature T_a and temperature difference ΔT between sensors. The temperature at each sensor is simply determined from $T_a \pm 1/2\ \Delta T$. The accuracies of the HFE temperature measurements are given in table 9-I.

The cable thermocouples consist of a string of four Chromel/constantan junctions embedded in each probe cable. The lowermost junction is positioned inside the gradient sensor housing at the top of the probe. The reference junction for each cable is inside the electronics housing and is mounted in an isothermal block with a platinum resistance thermometer (the reference thermometer). The thermocouple (TC) circuit is shown in figure 9-1(c).

The accuracy of the thermocouple measurements has special significance for interpreting the subsurface temperature profiles at the Apollo 17 site. Therefore, certain features of the thermocouple measurement, which affect the accuracy, should be described. First, only the Chromel/constantan junction (TC1) inside the topmost gradient is coupled with the reference junction during a measurement sequence. Junctions TC2, TC3, and TC4 are coupled with TC1 so that, in effect, TC1 becomes the reference junction and the

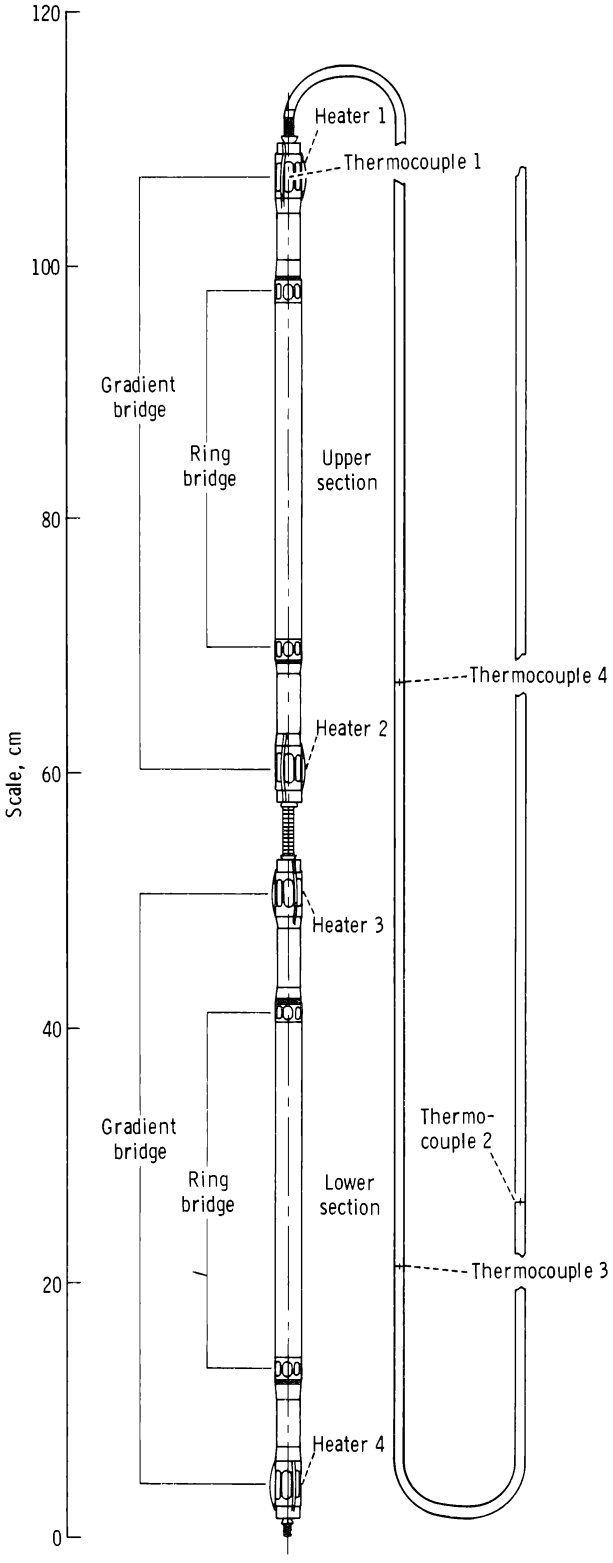

(a) Heat flow probe.

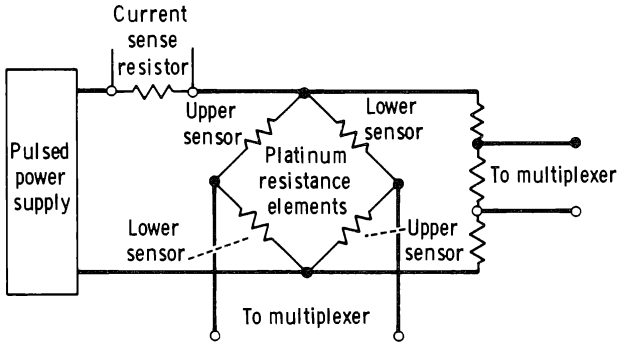

(b) Typical platinum resistance bridge circuit.

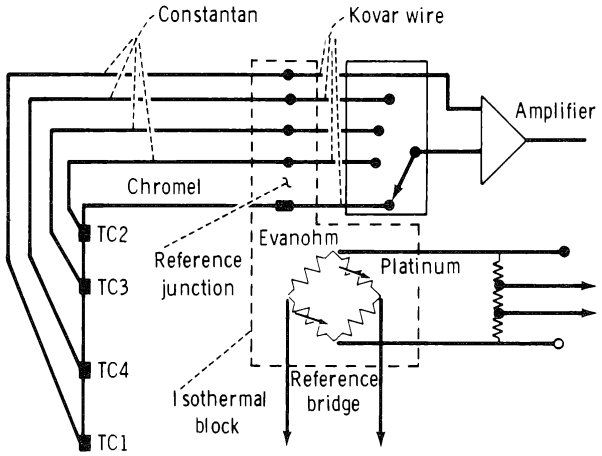

(c) Thermocouple circuit.

FIGURE 9-1.–Heat flow probe and circuits.

top gradient sensor becomes the reference thermometer. Because the temperatures of TC3 and TC4 are much closer to that of TC1 than to that of the thermometer in the electronics box, the calibration errors are reduced by this technique. Second, the placement of junction TC1 inside the gradient sensor permits a direct comparison between the two sensors on the Moon. Thus, an in situ calibration of the thermocouple circuit against the much more accurate gradient sensor is performed.

Conductivity experiments are made using 1000-ohm heaters that surround each of the gradient sensor housings. The experiments can be operated in either of two modes by energizing the heaters at 0.002 or 0.5 W, depending on the conductivity of the surrounding regolith. Because of the low conductivity of lunar material at Taurus-Littrow, only the lower power was used for the Apollo 17 conductivity experiment. After initiation, power is left on for 36

TABLE 9-I.–*Heat Flow Experiment Temperature Measurements*

Thermometer	*Temperature difference, K*		*Absolute temperature, K*	
	Range	*Accuracy*	*Range*	*Accuracy*
Gradient bridge (platinum resistance)[a]	± 2/± 20	± 0.001/± 0.01	190 to 270	± 0.05
Ring bridge (platinum resistance)	± 2	± .002	190 to 270	± .05
Cable thermocouples[b]	–	–	70 to 400	± .5
Reference thermometer (platinum resistance)	–	–	253 to 363	± .01

[a]Gradient-bridge temperature-difference measurements are made at two sensitivities with a ratio of 10 to 1.

[b]The stated accuracy applies when the top gradient sensor of each probe is used as the reference thermometer and when temperature differences between the junction and the top gradient sensor are less than 10 K. Approximately one-half of the stated error is due to uncertainties in determining the correction for the copper/Kovar junctions, which are in the thermocouple circuit.

hr or more, and the temperature rise of the sensor beneath the heater is precisely measured by the appropriate bridge. A more detailed description of the operation of the HFE can be found in reference 9-10.

Experiment Deployment at Taurus-Littrow

The HFE, deployed as part of the Apollo lunar surface experiments package (ALSEP), is located approximately 200 m west of the landing site. The electronics housing is located approximately 9 m north of ALSEP central station, and the two probes are emplanted approximately 5.5 m on either side of the electronics housing on approximately an east-west line. The ALSEP site is on a local topographic high, perhaps an intercrater ridge between two wide but shallow depressions north and southeast of the site. The two probes are emplanted near the rim of the shallow northern depression.

The borehole for probe 1 was drilled east of the electronics housing to a depth of 2.54 m, and the probe was inserted to 2.36 m, the maximum possible depth. The rim of a small, relatively recent crater, approximately 2 m in diameter and 0.3 m deep, lies approximately 1 m northwest of this borehole. Thermocouple TC12 is in a portion of the cable exposed above the surface. This portion of the cable, which is covered by a black sleeve, is oriented nearly north-south and is tipped up toward the south approximately 15° relative to the surface.

Probe 2 is buried in a borehole drilled west of the electronics housing to a depth of 2.55 m. The rim of a 3-m crater is approximately 2 m northwest of this probe site. Thermocouple TC22 is exposed above the surface, alined nearly north-south, and is almost level relative to the surface.

SUMMARY OF THE THEORY RELEVANT TO THE LUNAR HEAT FLOW MEASUREMENT

The important aspects of heat transfer that are essential to interpretation of the temperature and conductivity measurements are reviewed herein. For the reader primarily interested in the experiment results, this section may be used for reference only. The discussion is summary in nature; a more detailed description is available in references 9-11 and 9-12.

The Initial Cooldown of the Probe; Estimates of Thermal Conductivity of the Regolith and Equilibrium Temperatures

When the borestem is drilled into the soil and the probe is inserted, both are at temperatures considerably higher than their subsurface surroundings. The higher temperatures result from the temperature of these components above the surface before emplacement and from heat generated during drilling. Because of the complexity of the drilling process, it is difficult to estimate the amount of heat dissipated

and the distribution of heat along the borestem. Measurements made within minutes after the probes were inserted showed that the probes were approximately 40 to 50 K warmer than the surrounding undisturbed lunar soil. Because of the very low thermal conductivity of the lunar soil, this heat is dissipated very slowly. Even after 45 days, some of the thermometers indicated continued cooling.

In general, the rate of equilibration of each probe sensor to the surrounding lunar medium depends on several different parameters, including thermal and geometrical properties of the probe/borestem system, thermal properties of the adjacent lunar medium, the thermal contact between the borestem and the adjacent zone of disrupted lunar material, and the total heat energy excess of the system upon completion of drilling. For long times ($t > 20$ hr) after the probes are inserted, however, the probe sensor temperatures above equilibrium depend essentially on two quantities, the total initial energy excess per unit length of the system ΔE and the thermal conductivity of the adjacent regolith k_m.

$$T_p(t) - T_\infty = \Delta E/4\pi k_m t \qquad (9\text{-}2)$$

where $T_p(t)$ is a probe sensor temperature at time t since emplacement and T_∞ is the equilibrium sensor temperature.

The form of equation (9-2) has been verified by finite difference models and by analytical solution appropriate to simplified distribution of ΔE between the probe and borestem. The analytical solution, which takes the form of equation (9-2) for long times, is described in detail in the appendix of section 11 of reference 9-11.

Estimates of the regolith conductivity k_m can be made from the long-time cooldown data using equation (9-2) once a value for ΔE is assumed. Because of the uncertainties of the contribution of the drilling process to the total excess heat energy, two different assumptions have been made in regard to the ΔE term. First, it was assumed that drill-heating effects are negligible and that all excess heat energy initially resides in the probe and borestem. The probe and borestem were assumed to be at the same initial temperature T_0 after drilling, as measured by the probe sensors. For this assumption, the initial energy excess can then be expressed simply as

$$\Delta E = \left(S_p + S_b\right)\left(T_0 - T_\infty\right) \qquad (9\text{-}3)$$

where S_p and S_b are the heat capacities per unit length of the probe and borestem, respectively. The resultant problem has an analytical solution that is used to determine regolith conductivity estimates from the cooldown data. These assumptions constitute the minimum initial energy case.

For a maximum initial energy estimate, it was assumed that a 2.2-mm thickness of disrupted lunar material had received enough heat during the drilling process to attain an initial temperature equal to that of the probe and borestem. The 2.2-mm contact zone thickness was chosen to correlate with the difference in drill bit radius and borestem radius. The subsequent cooldown problem was then solved, assuming radial heat dissipation, by using a finite difference model. The curve-matching procedure was performed for times > 20 hr when all parameter effects, with the expection of k_m, were negligible; that is, when equation (9-2) was valid.

Because of the form of equation (9-2), the probe equilibrium temperatures can be estimated quite accurately independent of initial conditions and of k_m. By considering sensor temperatures T_{p1} and T_{p2} for times t_1 and $t_2 > 50$ hr, the unknown factor $\Delta E/4\pi k_m$ can be estimated from equation (9-2) to obtain

$$T_\infty = \frac{T_{p2} \times t_2 - T_{p1} \times t_1}{t_2 - t_1} \qquad (9\text{-}4)$$

Equilibrium temperature differences, measured by the platinum resistance bridges, can be calculated in a similar manner.

HEATER-ACTIVATED CONDUCTIVITY MEASUREMENTS

Because all eight conductivity measurements were made with a heater power of 0.002 W, the discussion is confined to this experiment mode. After the heat is energized, the temperature rise at the gradient sensor enclosed by the heater depends in a complex way on the thermal properties of nearby probe components, borestem, and lunar material, as well as the contact zones between these elements. A detailed finite difference model of the conductivity experiment at each heater location is used to interpret the temperature history of the gradient sensor in terms of the conductivity of material external to the borestem. Numerical model computations, laboratory experiments, and lunar experiments indicate that, for times

$>$ 20 hr, the temperature rise $\Delta T(t)$ is well defined by the simple relationship

$$\Delta T(t) = c_1 \ln(t) + c_2 \qquad (9\text{-}5)$$

where c_1 and c_2 are constants. The form of equation (9-5) is the same as that for a heated infinite cylinder in an infinite homogeneous medium at long times (i.e., $>$ 20 hr for a cylindrical source with a radius and heat capacity per unit length of the HFE probe/borestem system) (ref. 9-13).

For an infinite cylindrical source

$$c_1 = Q/4\pi k_m \qquad (9\text{-}6)$$

where Q is the power per unit length in W/cm. Thus, c_1 depends solely on the heater power per unit length and on conductivity. The constant c_1 can be determined easily because it is the slope of the temperature rise curve when plotted versus ln t; therefore, cylindrical sources are often used as a practical technique for measuring conductivity.

Conductivity is determined from lunar experiments by comparing observed slopes on a logarithmic time scale with values of c_1 calculated with the finite difference models. Parametric studies, in which certain thermal properties are varied singly in the numerical model, show that for times $>$ 20 hr, c_1 is very nearly insensitive to changes in pc of the surrounding medium, changes in borestem conductance, and changes in the thermal links between the probe and borestem and the borestem and lunar medium. However, c_1 is sensitive to changes in conductance in the probe body, which can alter the flow of heat from the heater axially along the probe. Assumptions of thermal properties in the numerical models that influence axial heat transfer along the probe are probably the largest source of error in the conductivity determinations.

The similarity in performance of the lunar conductivity experiment and of an infinite cylindrical source is principally due to the relatively efficient flow of heat axially along the borestem. Even though the probe heater is very short (1.9 cm), it heats a section of borestem that is long compared to the borestem diameter. For times $>$ 20 hr, the isotherms in the surrounding medium are roughly cylindrical in the vicinity of the heater as shown in figure 9-2. The numerical computations also show that the experiment is most sensitive to lunar material within approximately 5 cm of the borestem wall.

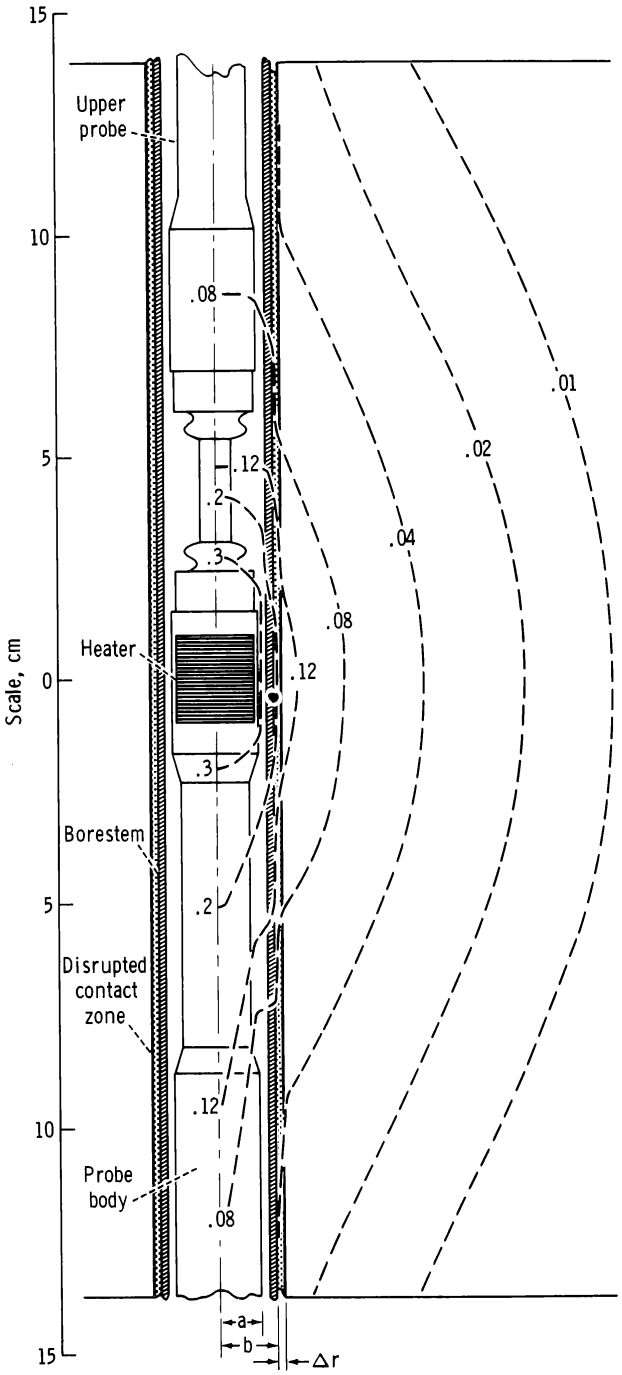

FIGURE 9-2.–The geometry of the probe, borestem, contact zone, and lunar regolith in the vicinity of a conductivity experiment. The dashed lines show surfaces of equal temperature rise in kelvins after the heater has been on for 36 hr. The model parameters are k_m = 2.4 × 10^{-4} W/cm-K and H_2 = 1.5 × 10^{-4} W/cm^2-K.

The effective conductance of the contact zone has a pronounced effect on the magnitude of the sensor temperature rise at any given time. Because k_m can

be determined independently, the conductance of the contact zone is the principal remaining unknown parameter and can be determined by matching observed and theoretical temperature curves for times > 0.5 hr.

Variations in Surface Temperature and Its Effect at Depth

Lunar surface temperatures vary nearly 300 K from just before lunar dawn to lunar noon. This variation induces subsurface variations that propagate downward as thermal waves. For a homogeneous medium of diffusivity α with a sinusoidal variation $A_o \cos \omega t$ at the surface, the temperature at a given depth z is given by

$$T(t,z) = A_o e^{-\delta z} \cos(\omega t - \delta z) \qquad (9\text{-}7)$$

where A_o is the amplitude of the surface variation in degrees, ω is the angular frequency in rad/sec (2.5×10^{-6} for the diurnal variation and 2×10^{-7} for the annual variation), and

$$\delta = \sqrt{\frac{\omega}{2\alpha}}, \ \text{cm}^{-1} \qquad (9\text{-}8)$$

Equation (9-7) indicates that the variation decreases in amplitude by a factor e^{-1} and is delayed in phase 1 rad for every δ^{-1} centimeters of depth.

The propagation of surface temperature variations into the lunar regolith is more complex for a number of reasons. First, the surface variation is not a simple sinusoid but contains significant higher harmonics. Second, thermal properties vary significantly with depth; and third, radiative transfer, which depends on T^3, plays an important role in the upper few centimeters of the lunar soil. It is necessary to resort to numerical calculations that include these complications to determine the expected temperature variations in the subsurface. In figure 9-3, the peak-to-peak attenuation and phase lag of the diurnal variation are shown as a function of depth for the conductivity profile at the Apollo 17 heat flow site. The upper part of the conductivity profile is derived from surface temperature measurements that are described in the section entitled "Surface Temperatures Deduced From Thermocouple Measurements." For depths greater than a few centimeters, the amplitude decreases in a simple exponential fashion, as evidenced by the nearly straight line on a semilogarithmic scale. Similarly, the phase lag shows a

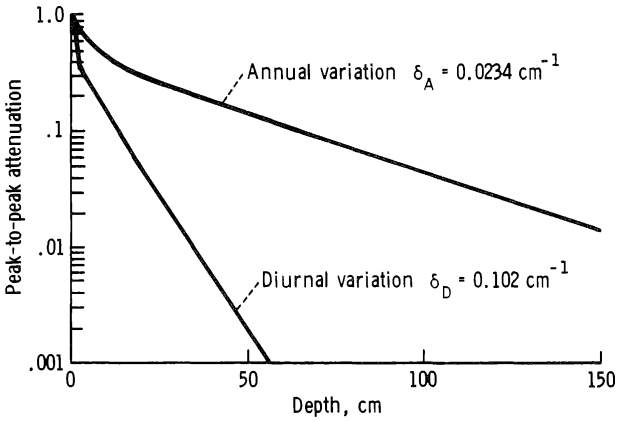

(a) The attenuation of the peak-to-peak amplitude of the diurnal and annual temperature with depth in the regolith. The δ in each equation is the effective decay constant deeper than 20 cm.

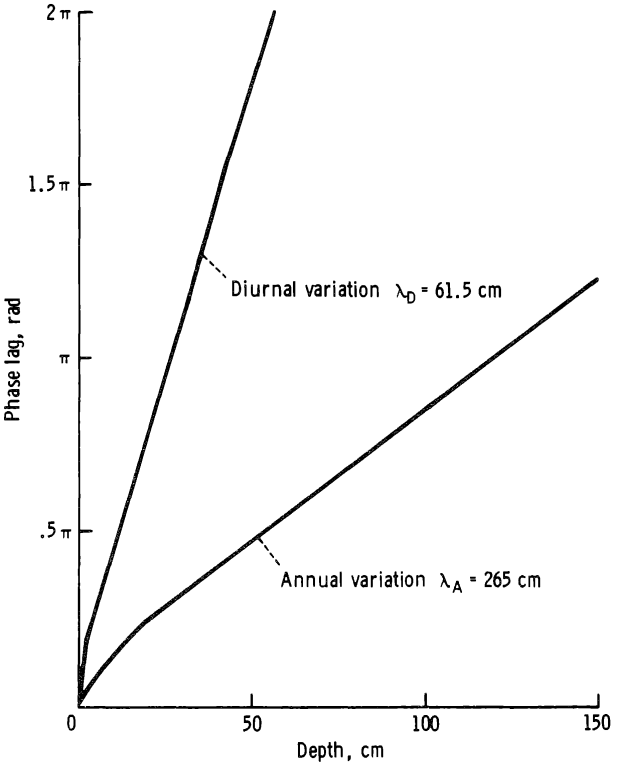

(b) Phase lag with depth. The values of λ are the wavelengths of the thermal wave below 20 cm. The model used for the diurnal variation is from Apollo 17 data. (See the section entitled "Surface Temperatures Deduced From Thermocouple Measurements.") The annual curves are calculated from a Rima Hadley thermal properties model (ref. 9-14).

FIGURE 9-3.–Peak-to-peak attenuation and phase lag as a function of depth.

nearly linear increase with depth below a few centimeters. Thus, the simple relationship of equation (9-7) would apply to a close approximation below these depths.

The temperature at lunar noon varies throughout the year because of the varying distance of the Earth-Moon system from the Sun. The noon temperature increases approximately 6 K from aphelion to perihelion. The mean temperature (i.e., surface temperature averaged over a lunation) varies approximately 3 K throughout a year. Although the amplitude of the annual cycle is one-hundredth of the diurnal variation, the decay constant δ is $\sqrt{12}$ times smaller; consequently, annual variations penetrate deeper and induce significant heat flows to depths of a few meters and must be considered in the interpretation of the experimental results. The attenuation of amplitude and the increase in phase lag for the annual wave are shown in figure 9-3 as a function of depth. Annual wave effects shown in figure 9-3 are based on the conductivity profile at Rima Hadley.

As shown in figure 9-3, temperature fluctuations attributable to the diurnal cycle become virtually undetectable at depths > 100 cm and would have had little effect on heat flow below this depth before the probe and borestem were emplaced. Once the borestem is emplanted in the regolith, the higher conductivity of the borestem and the radiative transfer inside the borestem will enhance the downward propagation of thermal waves. However, thermometers at 130 cm below the surface do not detect any temperature variation during a lunation cycle.

Corrections for the Shunting Effects of the Borestem and Probe

The axial conductance of the epoxy borestem is considerably higher than that of a vertical column of lunar soil of equal cross section. This fact, combined with the finite length of the borestem, results in some shunting of the steady-state heat flow through the borestem to the surface. Certain short sections of the borestem, such as the bit and joints, are made of titanium or steel, and sizable disturbances occur near these parts. A second related effect results from the fact that the probes are radiatively coupled to the borestem walls and have a small axial conductance. Consequently, the probe bridges register slightly smaller temperature differences than those registered at points on the borestem next to sensors.

These effects can be estimated by simplified analytical models and by laboratory experiments; both methods were used in the earlier analysis of the Apollo 15 results. However, for the Apollo 17 analysis and the refined Apollo 15 results presented in this report, a numerical model of the probe in a medium in which heat is flowing parallel to the probe axis has been used. The numerical model is more detailed and allows examination of certain combined effects that are difficult to estimate with analytical models.

The numerical model computations show that the borestem and probe disturbances to the steady-state heat flow are small. In the extreme case, the temperature difference across a probe section is 7 percent lower than the temperature difference across the same vertical distance interval far from the borestem. The numerical model has been used to apply corrections to all probe observations.

RESULTS

Apollo 17 Subsurface Temperatures

The HFE was turned on while probe 2 was being inserted into the borestem, and temperatures were recorded only minutes after drilling was completed. These temperatures ranged from 295 to 301 K. The early cooling histories of probe 1 indicate similar initial temperatures. After emplacement, the probes cool toward the undisturbed regolith temperatures. The temperature histories of all sensors deeper than 65 cm for the first 45 days are shown in figure 9-4. After 45 days, some sensors are continuing to cool; however, the expected future temperature decrease is probably less than the error of absolute temperature measurement.

The equilibrium temperature differences and the absolute temperatures of each sensor are listed in table 9-II. The correction for the steady-state disturbance of the heat flow by the borestem and probe system is applied to temperature data listed under the headings entitled "Corrected temperature difference" and "Corrected temperature." The appropriate corrections of the temperature difference attributable to the annual thermal wave during January 1973 (listed in the far right column) have not been applied because they are based on the conductivity profile at Rima Hadley. Note that the largest correction is approximately -4 percent.

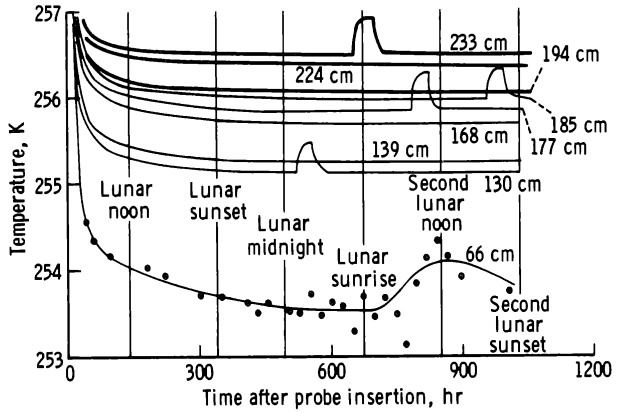

(a) Probe 1 (TC14).

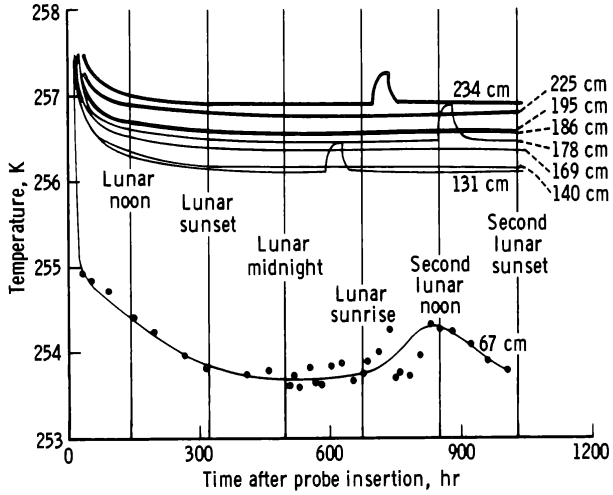

(b) Probe 2 (TC24).

FIGURE 9-4.–Apollo 17 temperature histories of all sensors 65 cm or deeper. The short pulses appearing on some of the sensor traces result from heater initiation for conductivity experiments. The numbers on each curve refer to the depths below the surface. The lowermost curves on each plot are TC4 thermocouple measurements. Some representative data points from the thermocouples are shown to indicate the scatter of these measurements. Temperatures shown are calculated by subtracting TC1 values from those of TC4 and adding them to the top gradient sensor temperature. The corrections given in table 9-III have not been added.

Temperature measurements of thermocouples TC14 and TC24 are also shown in figure 9-4. Some randomly sampled representative points are shown, and the solid curve is fitted visually to show the trend. The standard deviation of the points around the smoothed curve is approximately 0.3 K during the day and about half that value during the night. The values shown are calculated by subtracting the temperature at TC1 from that at TC4 and adding the result to the temperature at the top gradient sensor.

Comparison of the temperatures measured by TC11 and TC21 with those at the top gradient sensors shows relatively large errors in absolute temperature measurement (table 9-III). The source of these errors has been traced to the copper/Kovar (Cu/Ko) junctions, in each thermocouple electronics circuit, that are mounted on circuit boards in the electronics housing. The errors are proportional to temperature differences between the Cu/Ko junctions. Thus, the errors in TC11 and TC21 are direct measures of this temperature difference and can be used to estimate errors at all junctions. The larger errors during the night result from larger temperature gradients across the Cu/Ko junctions at night, and the larger errors at probe 2 junctions are caused by the greater distance between the Cu/Ko junctions in the probe 2 circuit. A preliminary analysis of electromotive forces produced by Cu/Ko junctions was used to calculate the corrections that should be applied to the data in figure 9-4. These corrections virtually erase the apparent variation between night and day measurements. The corrections have been applied to the data compiled in table 9-II. The uncertainty of determining these corrections is estimated as ± 0.4 K. Studies of the accuracies of the thermocouple measurements are continuing.

The thermocouple temperatures given in table 9-II represent the averages of the values obtained during the time from lunar sunset of the first day to lunar sunset of the second day. The amplitude of the diurnal variation at 66 cm cannot be determined with the present accuracy of the data (± 0.5 K).

In figure 9-5, the equilibrium temperatures are plotted as a function of depth. Temperatures along the body of probe 1 show a steady decrease in gradient with depth. The gradient decreases from 0.016 K/cm in the depth range 130 to 177 cm to 0.012 K/cm in the range 185 to 233 cm. This decrease is principally due to a general increase in conductivity of the regolith over the interval of measurement. The thermocouple temperature indicates a gradient of 0.013 K/cm from 66 to 130 cm; however, the accuracy of this measurement is poor.

At probe 2, the probe thermometers at a depth range of 131 to 234 cm indicate a rather uniform

TABLE 9-II.–*Apollo 17 HFE Subsurface Temperature Data*

(a) Temperature difference measurements

Bridge	*Interval, cm*	*Equilibrium temperature difference, K*[a]	*Corrected temperature difference, K*[b]	*Annual wave correction, K*
Probe 1				
DTG11	130 to 177	0.707	0.755	− 0.027
DTR11	139 to 168	.435	.467	− .018
DTG12	185 to 233	.533	.559	− .001
DTR12	194 to 224	.322	.326	< .001
Probe 2				
DTG21	131 to 178	.370	.390	− .027
DTR21	140 to 169	.218	.223	− .018
DTG22	186 to 234	.336	.359	− .001
DTR22	195 to 225	.206	.212	< .001

[a]The error associated with extrapolating to equilibrium temperature differences is ± 0.003 K.
[b]The uncertainty introduced by these corrections is estimated to be ± 2 percent.

(b) Absolute temperature measurements

Sensor type	*Depth, cm*	*Equilibrium temperature, K*[a]	*Corrected temperature, K*[b]
Probe 1			
Thermocouple TC4	66	254.20	254.20
Platinum resistance	130	255.06	255.02
Platinum resistance	139	255.19	255.17
Platinum resistance	168	255.62	255.64
Platinum resistance	177	255.76	255.78
Platinum resistance	185	255.91	255.91
Platinum resistance	194	256.03	256.04
Platinum resistance	224	256.36	256.37
Platinum resistance	233	256.44	256.47
Probe 2			
Thermocouple TC4	67	254.70	254.70
Platinum resistance	131	256.07	256.05
Platinum resistance	140	256.09	256.09
Platinum resistance	169	256.31	256.31
Platinum resistance	178	256.44	256.44
Platinum resistance	186	256.48	256.48
Platinum resistance	195	256.52	256.51
Platinum resistance	225	256.73	256.73
Platinum resistance	234	256.82	256.84

[a]The accuracy of extrapolated absolute temperatures is ± 0.05 K for the platinum resistances.
[b]The correction for the annual wave to be applied to the thermocouple is 0.04 K.

gradient of 0.0078 K/cm, whereas the gradient between 67 and 131 cm is 0.021 K/cm, a change by a factor of approximately 3. This large variation of gradient can be accounted for only partially by the variation of conductivity of the regolith immediately surrounding the borestem.

Apollo 15 Subsurface Temperatures

Subsurface temperatures measured at Rima Hadley below the depth disturbed by diurnal variations were reported in reference 9-11 without correction for the annual wave. In addition, corrections for the bore-

TABLE 9-III.–*Errors and Corrections in Absolute Temperature Measurements*

Sensor	*Lunar day*	*Lunar night*
Error (compared with top gradient sensor TC1), K		
TC11	1.1	1.9
TC21	1.4	2.5
Estimated corrections,[a] K		
TC14	0.4	0.7
TC24	.6	1.2

[a]The uncertainty in determining these corrections is estimated as ± 0.4 K.

stem and probe disturbance were derived from much simpler models than those discussed herein. Temperatures measured at longer times after probe insertion are now available, and a more accurate determination of equilibrium temperatures is possible. The temperatures and temperature differences at four sensors on probe 1 at Rima Hadley are presented in table 9-IV. More accurate corrections for the borestem disturbance and a correction for the annual wave effect have been applied. These measurements will be the basis for a slightly revised heat flow value.

Conductivity Estimates from Cooldown Analysis

Because of the uncertainties in the total heat energy associated with drilling, two cases assuming different initial conditions have been examined. These cases have been described in the preceding section on theory. Results derived assuming initial borestem and contact zone temperatures to be equal to the initial probe sensor temperature are listed in table 9-V under the heading entitled "Conductivity with drill heating effects." Conductivity estimates derived assuming that only the borestem and probe were initially at elevated temperatures are listed under the heading entitled "Conductivity without drill heating effects." The two cases are considered to be bracketing assumptions of the actual initial conditions. Cooldown conductivity estimates were made for each of the eight sensors along each probe. Additionally, cooldown analyses were performed assuming drill heating effects for the thermocouples located 65 cm above each probe.

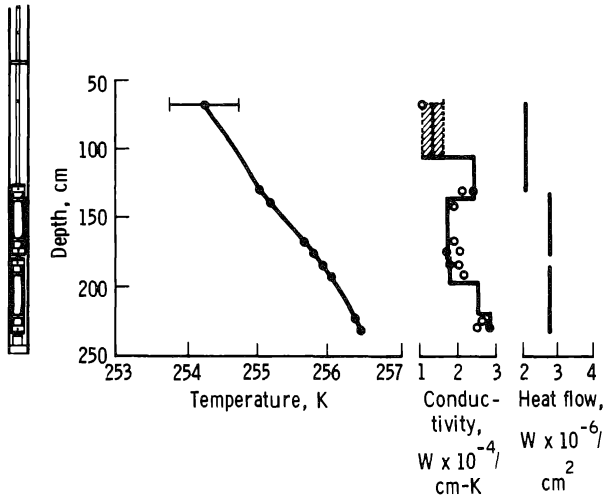

(a) Probe 1.

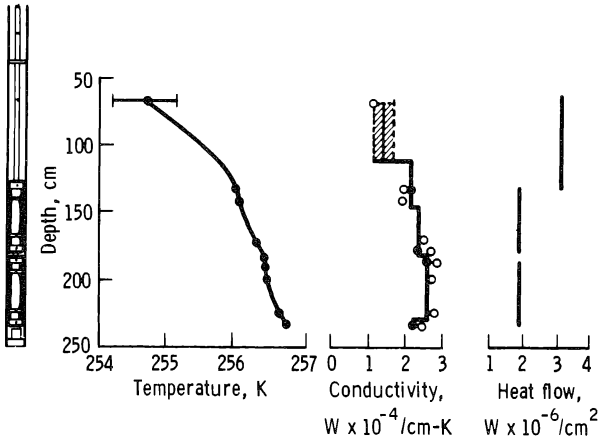

(b) Probe 2.

FIGURE 9-5.–Equilibrium temperatures, conductivities, and heat flows measured by the Apollo 17 probes. The open circles on the conductivity plot are calculated from cooldown curves assuming maximum drilling energy, and the solid circles are heater-activated experiment results. The solid line represents a layered model used for calculating heat flow. In the heat flow figure, the solid lines give heat flow over the three largest intervals. The geometry of the probe in the subsurface is shown at the far left.

The large noise on the thermocouple data limits the accuracy of conductivities deduced from the cooling history. Deductions of the conductivity at depths from 3 to 15 cm below the surface, which will be discussed later in this section, give values of approximately 1.2×10^{-4} W/cm-K. Based on these results at shallow depths, we estimate the conductivity lies in the range 1.0×10^{-4} to 1.6×10^{-4}

TABLE 9-IV.–*Apollo 15 HFE Subsurface Temperature Data*

(a) Temperature difference measurements

Bridge	*Interval, cm*	*Equilibrium temperature difference, K*	*Corrected temperature difference, K*[a]	*Annual wave correction, K*
Probe 1				
DTG12	91 to 138	0.803	0.833	− 0.37
DTR12	100 to 129	.484	.479	− .28

(b) Absolute temperature measurements

Sensor type	*Depth, cm*	*Equilibrium temperature, K*	*Corrected temperature, K*
Probe 1			
Platinum resistance	91	252.20	252.16
Platinum resistance	100	252.33	252.33
Platinum resistance	129	252.81	252.81
Platinum resistance	138	253.00	253.01

[a]The effect of the annual wave on Sept. 29, 1971, has been removed.

TABLE 9-V.–*Conductivities from Cooldown Histories*

Sensor depth	*Heater location*	*Conductivity with drill heating effects, $W \times 10^{-4}$/cm-K*	*Conductivity without drill heating effects, $W \times 10^{-4}$/cm-K*
Probe 1			
66		1.0	–
130	H11	2.3	1.3
139		1.9	1.1
168		1.9	1.1
177	H12	2.0	1.0
185	H13	1.9	1.1
194		2.1	1.1
224		2.8	1.4
233	H14	2.7	1.6
Probe 2			
67		1.0	–
131	H21	2.0	1.2
140		2.0	1.1
169		2.4	1.3
178	H22	2.7	1.7
186	H23	2.9	1.7
195		2.7	1.5
225		2.8	1.5
234	H24	2.5	1.5

W/cm-K at 66 cm. This range is indicated in figure 9-5.

By comparison with the more accurate heater-activated conductivity determinations discussed in the next section, it is evident that drill heating effects cannot be neglected if reliable conductivity information is to be extracted from the cooldown data. When substantial drill heating effects are included in the cooldown analyses, conductivity determinations and variations with depth agree well with the heater-activated conductivity experiment results. The cooldown conductivity estimates are particularly valuable in interpolating between the more accurate heater-activated conductivity determinations.

Heater-Activated Conductivity Experiments

Conductivity experiments at each of the eight heater locations have been performed. Figure 9-6 shows the sensor temperature rise history and theoretical curves for one such experiment. The conductivities k_m and contact conductances H_2 are given in table 9-VI. These results and the cooldown estimates with drill heating effects are shown in figure 9-5. It is clear that the conductivity does not vary in any simple way with depth.

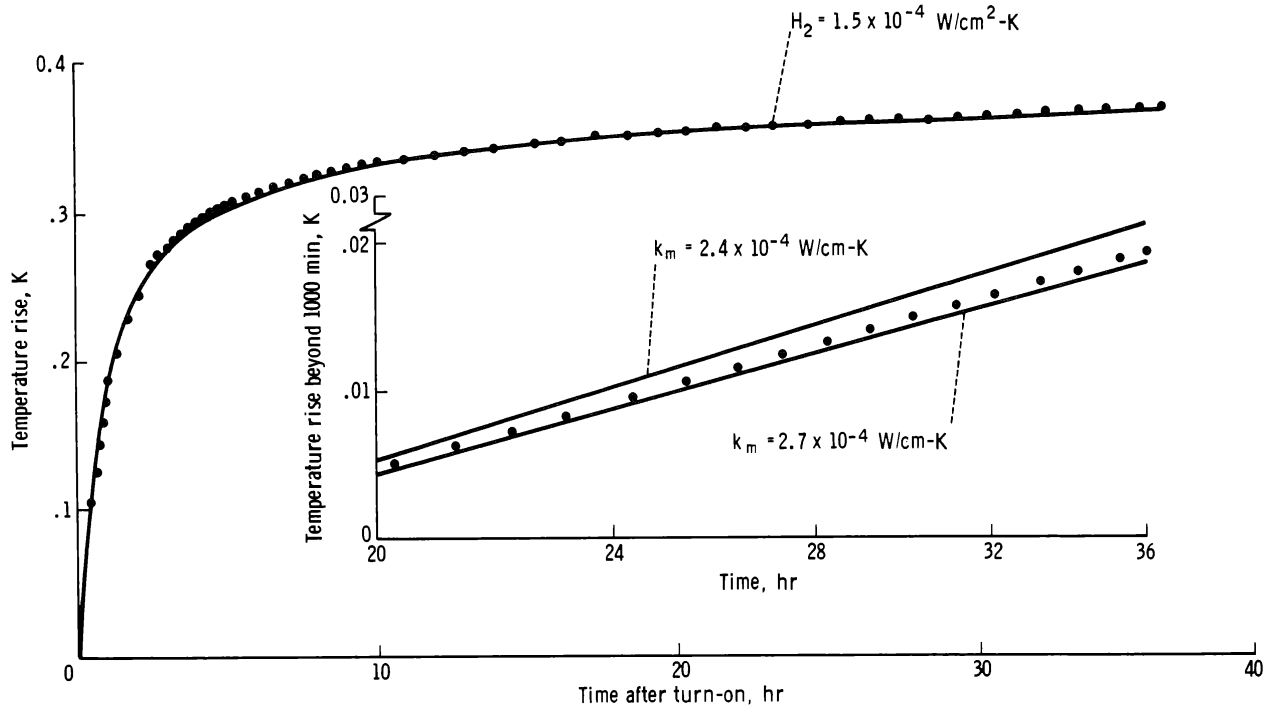

FIGURE 9-6.–Temperature rise during a conductivity experiment (dots) is compared with a theoretical curve derived from a model with k_m = 2.7 × 10^{-4} W/cm-K and H_2 = 1.5 × 10^{-4} W/cm^2-K. In the inset, the temperature rise for times > 1000 min is shown on an expanded scale plotted against the logarithm of time. The observed data are compared with two bracketing theoretical curves. The reduced conductivity is 2.64 W/cm-K.

A rough correlation exists between the drill penetration rate during borestem drilling and the measured conductivity. The more resistant layers where the drill penetrated slowly correspond to depths where higher conductivity is observed. The more resistant layers likely correspond to more compacted regolith materials or possibly to a higher concentration of centimeter-size rock fragments. Either of these phenomena can increase the bulk conductivity. The relatively high conductivity measured at 130 cm on probe 1 lies within a zone from 80 to 130 cm where penetration was slow. Directly below this layer, drilling rates were relatively high and the conductivity values are correspondingly lower. These correlations are used to interpolate values between discrete measures. In figure 9-5, the solid line that passes through the heater-activated conductivity values represents a layered model of conductivity in the regolith based partly on penetration rates and partly on cooldown estimates. At probe 2, some of the drilling operation was not visually monitored so that correlations with conductivity cannot be made during the unmonitored period, which includes approximately half the depth range where probe 2 is emplaced.

One interesting feature of these conductivity results is a rather large difference between the conductivity profiles at probe 1 and probe 2. It is possible that layers, as defined by conductivity, have some dip relative to the surface. For example, the high conductivity layer at 100 cm at probe 1 could correspond to the high conductivity layer between 170 and 230 cm at probe 2.

The contact conductance H_2 arises from low conductivity material lying in a disturbed zone just outside the borestem. We estimate this zone to be 2.2 mm thick. The conductivity k_c of material in the contact zone is given by

$$k_c = H_2\left(b + \frac{\Delta r}{2}\right)\ln\left(\frac{b + \Delta r}{b}\right) \qquad (9\text{-}9)$$

(See fig. 9-2 for definition of parameters in this equation.) As an example, for H_2 = 1.4 × 10^{-4} W/cm^2-K, k_c = 3.0 × 10^{-5} W/cm-K. This value of conductivity is approximately a factor of 6 less than that of the surrounding regolith.

TABLE 9-VI.–*Results of the Conductivity Experiments*

Heater location	*Depth, cm*	*Conductivity,*[a] $W \times 10^{-4}$ */cm-K*	*Contact conductance,*[b] $W \times 10^{-4}$ */cm²-K*
Apollo 17 probe 1			
H11	130	2.50	1.4
H12	177	1.72	1.6
H13	185	1.79	1.4
H14	233	2.95	1.2
Apollo 17 probe 2			
H21	131	2.06	1.6
H22	178	2.36	1.1
H23	186	2.64	1.5
H24	234	2.24	2.3
Apollo 15 probe 1			
H11	35	1.41	0.8
H12	83	2.11	.8
H13	91	1.60	.9
H14	138	2.50	1.0
Apollo 15 probe 2			
H23	49	1.46	0.5
[c]H24	96	2.43	.6

[a]The estimated error of conductivity measurement is ± 15 percent.

[b]Estimated error is ± 20 percent. In the theoretical model the thickness of the contact zone is 2 mm.

[c]It is probable that a section of broken borestem lies just outside this location so that the uncertainty of this measurement is very large.

Apollo 15 Results

Six conductivity experiments using a heater power of 0.002 W were performed on the Apollo 15 probes. The analyses of three of these measurements were not described in reference 9-11 because it was very difficult to separate changes attributable to heater turn-on from large diurnal variations in temperature. Subsequently, two of the measurements have been repeated at times in the lunation when the rate of temperature change at the heater location was minimal. In addition, the diurnal temperature variation from preceding and succeeding lunations is available to help interpolate trends during the time that the heater is on. Lastly, some refinements have been made in the finite difference models of the conductivity experiments. The newer models indicate small adjustments in the previously published values. The revised Apollo 15 conductivity values at each heater location are given in table 9-VI.

Heat Flow

The magnitude of the vertical component of heat flow in the regolith can be calculated from the temperature and conductivity profiles in figure 9-5. Over each depth interval z_1 to z_2

$$F_z = k_{ave} \frac{\Delta T_{z_1 - z_2}}{z_2 - z_1} \qquad (9\text{-}10)$$

where $\Delta T_{z_1 - z_2}$ is the corrected temperature difference listed in tables 9-II and 9-IV and k_{ave} is the average conductivity in the depth interval $z_1 - z_2$ calculated from the layered models in figure 9-5.

Gradients, average conductivities, and heat flows calculated from the Apollo 15 and Apollo 17 results are presented in table 9-VII. The heat flow data over the entire depth range of temperature measurement

TABLE 9-VII.–*Heat Flow Data*

Depth interval, cm	*Temperature gradient, K/cm*	*Average conductivity,* $W \times 10^{-4}$ */cm-K*	*Heat flow,* $W \times 10^{-6}$ */cm²*
Apollo 17 probe 1			
66 to 130	0.0130	1.60	2.10
130 to 177	.0158	1.79	2.83
139 to 168	.0163	1.72	2.80
185 to 233	.0118	2.39	2.81
194 to 224	.0113	2.48	2.81
66 to 233	.0140	1.80	2.50
Apollo 17 probe 2			
67 to 131	0.0210	1.50	3.10
131 to 178	.0082	2.26	1.86
140 to 169	.0078	2.30	1.79
186 to 234	.0076	2.50	1.89
195 to 225	.0074	2.53	1.87
67 to 234	.0130	2.00	2.50
Apollo 15 probe 1			
91 to 138	0.0175	1.78	3.11
100 to 129	.0166	1.68	2.82

are presented on the bottom lines of table 9-VII for Apollo 17 probes 1 and 2. At probe 1, the most representative value of heat flow (2.8×10^{-6} W/cm^2) is thought to be that determined by the probe data over the interval 130 to 233 cm. At probe 2, the measurement is possibly disturbed, as will be discussed in the next section, and the most representative value (2.5×10^{-6} W/cm^2) is that calculated using data between 67 and 234 cm. The heat flow calculated over the interval 91 to 138 cm is believed to be the best value from the Apollo 15 measurements.

At the Apollo 17 probe 1 site, the heat flow is quite uniform over the entire depth range. The variation falls well within the estimated error of measurement. Probe 2 results show a uniform heat flow along the length of the probe, but heat flow between 67 and 131 cm is 70 percent greater. The large change in gradient is partly compensated for by an increase in conductivity with depth. The overall heat flow of 2.5×10^{-6} W/cm^2 is in fair agreement with the probe 1 value of 2.8×10^{-6} W/cm^2.

DISCUSSION OF HEAT FLOW RESULTS

The Probe 2 Measurements

The change in heat flow at probe 2 by a factor slightly less than 2 over the depth range of 67 to 234 cm is most reasonably explained by refraction of heat flow in the vicinity of a large buried boulder. A relatively large number of rocks are strewn over the ALSEP area. Lunar basalts have conductivities of approximately 1.2×10^{-2} to 1.8×10^{-2} W/cm-K at 250 K (ref. 9-15). These values are 60 to 90 times the conductivity of the fine-grained regolith material. Thus, large blocks of solid rock in the subsurface can result in significant shunting of heat flow.

To illustrate the shunting effect, the distortion of heat flow lines and isotherms around and through a square of material having 60 times the conductivity of a surrounding infinite medium is shown in figure 9-7. The model is two-dimensional and symmetric at the left margin of the figure. One significant feature of the model is that very little effect is evidenced at distances greater than one-half of the width of the rock. Thus, heat flow measurements would have to be made quite close to a rock (less than one-fourth of the width) to detect a disturbance as large as that at probe 2. However, probe 2 must be more than 5 cm from a rock in order for the rock not to have a detectable effect on the heater-activated conductivity experiments.

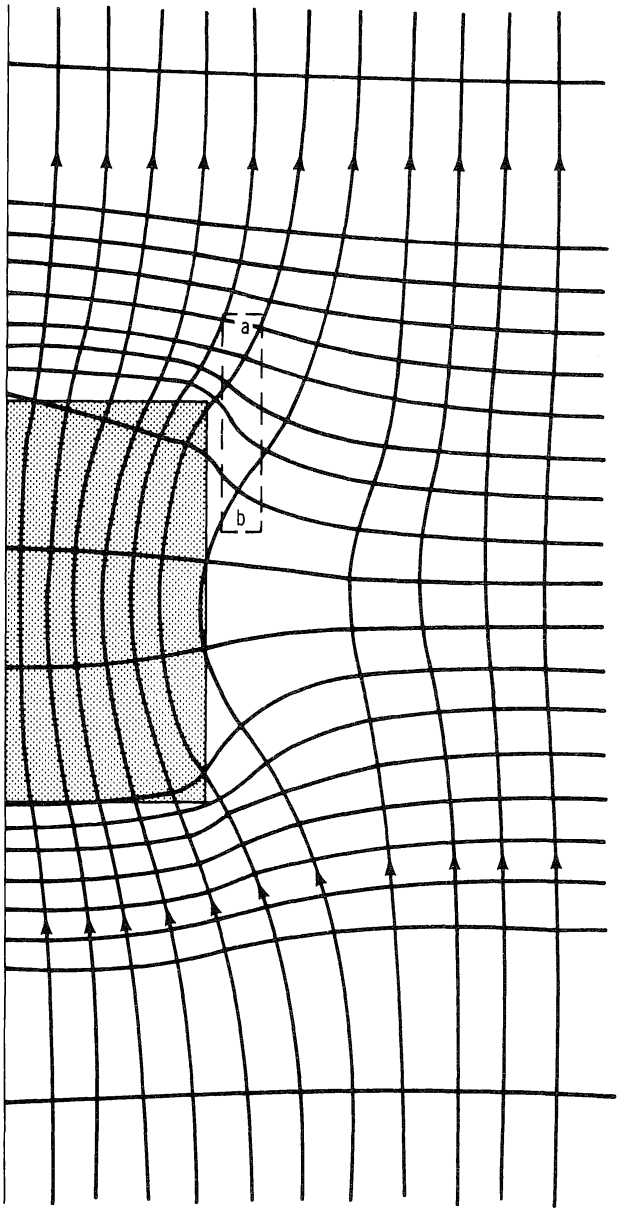

FIGURE 9-7.–The effect of a square of material on vertical heat flow (shaded area) which has a conductivity 60 times that of the surrounding material, shown by the distortion of isotherms and flow lines. These results are based on a finite difference model computation.

If probe 2 were located relative to a large subsurface boulder in a zone defined by the dashed rectangle in figure 9-7, a temperature profile similar to that observed would result. Other features such as

the slightly higher absolute temperatures measured by probe 2 relative to probe 1 at all depths would also be explained. It should be noted that to explain the rather sudden change in gradient shown in figure 9-5, a rather sharp-cornered rock is required.

If the vertical gradient were calculated using the temperature difference between points a and b in figure 9-7, the result would not be much different than the vertical gradient far from the rock. This result is obtained because the measurement interval is large enough to span the zone of dilation of isotherms adjacent to the rock and the compensating zone of compression of isotherms above it. If the same is true for probe 2, then the gradient determined by using temperature points at 67 and 234 cm should be close to the regional value. The fact that the average gradient at probe 2 is in close agreement with results of probe 1, which is thought to be free of such disturbances, supports this possibility. The results of probe 1 should be regarded as the more representative value of heat flow at Taurus-Littrow.

The Effects of Topography

Detailed assessment of the effects of topography on the Taurus-Littrow measurement has not been completed to date. However, some idea of the magnitude of expected disturbances can be made based on simplified terrain models. There are two important effects of topography on the Moon. First, surface relief causes a distortion of subsurface isotherms to conform to the surface temperature distribution. Consequently, a lowering of regional heat flow is generally found over convex-up features and an augmentation of heat flow is found over concave-up features. Second, lunar topography has a significant effect on the surface temperature distribution because the mean surface temperature depends on a radiative balance of solar flux, radiation to space, and reradiation from the surrounding lunar surface. In general, depressions such as craters will have slightly elevated mean temperatures because of the decreased view of the crater floor to space and reradiation from other parts of the crater (ref. 9-16). However, a north-facing slope such as that of the South Massif would have a lower mean temperature because of the relatively large angle of incidence of solar rays throughout the lunar day.

Craters of all sizes greater than 1 m in diameter that are within a distance of one crater diameter could have a measurable effect on the heat flow measurement. For example, the small craters near probes 1 and 2 must be considered as well as the 600-m crater Camelot approximately 600 m to the east of the ALSEP site. Most of these craters have an aspect ratio (diameter over depth) of approximately 6 to 1. The dominant effect of such craters is to increase heat flow in areas just outside the rim because of the slightly higher mean surface temperature inside. Finite difference models show that the excess heat flow decreases very rapidly with distance from the crater rim. At one crater radius from the rim of a crater having a floor that is 3 K warmer than the surrounding flat surface, heat flow is increased approximately 0.1 W/cm^2. Because the heat flow probes are one or more radii away from the rims of all craters of interest, the combined effect of all craters would be small. An estimate of 0.3 W/cm^2 or 10 percent would be conservative. The important result is that a negative correction must be applied to the observed values in order to compensate for nearby craters.

The valley floor at Taurus-Littrow, aside from craters, is relatively smooth, and only the mountain ranges north and south of the site would have significant effects. The effect of the massifs can be estimated using a method developed by Lachenbruch (ref. 9-17). The valley at Taurus-Littrow is modeled as a flat-floored trough in an otherwise flat surface. The walls of the trough have uniform slopes equal to the average slopes of the north and south massifs measured from topographic maps. Lachenbruch has published tables from which an estimate can be made of the effect on heat flow of such sloping surfaces intersecting horizontal planes. Based on this model, the topographic effect of the massifs will cause a 20-percent increase in heat flow at the ALSEP site. This estimate is maximal because it assumes that the trend of the ridges extends infinitely at the maximum elevation. The effect of the South Massif, in particular, is overestimated because the ridge does not extend very far to the southeast of the ALSEP site.

Last, the valley at Taurus-Littrow would have a slightly greater mean temperature (approximately 1 to 2 K) than the surrounding regions because the valley behaves radiatively like a crater. The flow of heat from the warmer valley floor to the surface outside the bounding massifs would tend to decrease the heat flow in the valley. This effect, which has not been quantitatively estimated at this time, may be

significant and would tend to counterbalance the positive effects already described.

In summary, the preliminary analysis of the effect of topography on the Apollo 17 measurement indicates that a negative correction estimated at 15 to 25 percent should be applied to this observation. However, we believe that a more detailed and careful analysis should be made before it can be assumed that effects of topography result in a significant difference between the heat flow measurements at the Taurus-Littrow and Rima Hadley sites.

Possible Correlation with Surface Radioactivity

As previously described, a correction for the gross effects of topography of approximately −20 percent might be applicable to observed heat flow at Taurus-Littrow, which would result in a value approximately 25 percent less than that measured at Rima Hadley. Because the difference depends on the topographic correction, its significance may be questionable. However, taken at face value, there is a correlation between the heat flow at the two sites and the surface radioactivity, as measured by the Apollo 15 gamma ray spectrometer (ref. 9-18). Relatively high thorium abundances were observed over the southeast corner of Mare Imbrium, and appreciably smaller abundances were observed over the southeast corner of Mare Serenitatis. The gamma ray spectrometer is sensitive only to the gamma-ray-emitting isotopes of uranium, thorium, or potassium in the most superficial layer. This tentative correlation with the heat flow measurement, which detects the integrated effects of radiogenic heating to depths of approximately 300 km, indicates that the surficial variations may extend to depth. It further suggests that the variation of surface radioactivity may be the best available indicator of the variation of heat flow over the lunar surface. However, these conclusions are tentative and must await a more thorough analysis of topographic effects.

Comparison with Earth-Based Microwave Measurements

Before the in situ measurements of Apollo 15 and 17 were obtained, estimates of the lunar heat flow had been made based on centimeter wavelength observations of the natural emission of the Moon, as cited in references 9-7 to 9-9. The lunar regolith becomes increasingly transparent at wavelengths beyond the infrared. Thus, observations at longer wavelengths yield temperature information at increasing depths into the lunar regolith. For wavelengths greater than approximately 5 cm, the effective emitting layer is far enough below the lunar surface that no variation in apparent brightness temperature over a lunation can be detected. However, an increase in brightness temperature with increasing wavelength has been observed. A plot of these measurements is given in reference 9-9. Between 5 and 20 cm, a nearly linear increase of brightness temperature $T_b(\lambda)$ with wavelength λ yields an average spectral gradient of $\partial T_b/\partial\lambda$ = 0.8 K/cm. To interpret the spectral temperature gradient in terms of a heat flow, estimates must be made of the electrical properties and of the thermal conductivity k of the effective emitting layer for the 5- to 20-cm waves. In particular, the characteristic penetration depth $\ell_e(\lambda)$ of an electromagnetic wave must be known as a function of wavelength.

Tikhonova and Troitskii (ref. 9-9) used simplified models of thermal and electrical property profiles to explain the microwave data over the 5- to 50-cm spectral range. The resultant inferred heat flow values of 2.9×10^{-6} to 4.0×10^{-6} W/cm are in remarkable accord with the in situ Apollo measurements, considering the approximations and assumptions necessary to the remote determination. In particular, the electrical and thermal parameters were estimated from observations applicable only to depths characterized by diurnal temperature variations. The assumption that near-surface parameter values apply to meter depths could lead to significant errors in the interpretation of the observed spectral gradient. Electrical property determinations based on remote radar measurements and on measurements made on returned lunar samples must be used to interpret the measured spectral gradient in terms of a thermal gradient. If the electrical and thermal properties of the regolith are considered to be homogeneous for depths greater than approximately 70 cm and extend at least 5 to 10 m, the thermal temperature gradient can be expressed in terms of the spectral gradient by

$$\frac{\partial T}{\partial z} = \frac{\lambda \partial T_b/\partial \lambda}{(1 - R)\ell_e} \tag{9-11}$$

where R is the appropriate centimeter wave reflec-

tion coefficient for the lunar-surface/space interface.

For the very low electrical conductivities found in the lunar regolith, the electromagnetic penetration depth $\ell_e(\lambda)$ may be written for the centimeter wave spectral region as

$$\ell_e(\lambda) = \lambda/(2\pi\sqrt{\epsilon}\ \tan\ \Delta) \qquad (9\text{-}12)$$

where ϵ is the dielectric constant and tan Δ is the loss tangent at centimeter wavelengths.

The average temperature gradient of 0.017 K/m measured in situ at the Apollo 15 and 17 sites would produce the observed spectral gradient if $\sqrt{\epsilon}$ tan $\Delta \cong$ 0.003, assuming R = 0.05. The feasibility of such a value for $\sqrt{\epsilon}$ tan Δ is supported by direct surface observations in the 0.4- to 3-cm wavelength range (ref. 9-19). Direct measurements of returned Apollo samples over a wide range of frequencies indicate a dielectric constant for the regolith material in the range 2.2 to 3.2 that is nearly frequency independent. However, loss tangent measurements yield values in the range 0.0004 to 0.01 and are frequency dependent (refs. 9-20 and 9-22). Additional electrical property measurements and refined analysis of the existing data on regolith samples must be made before the thermal gradient measured in situ can be supported on a moonwide basis by the spectral gradient observations.

The Representativeness of the Two Heat Flow Measurements

The regional geological settings of Rima Hadley and Taurus-Littrow are quite similar. Both are located on lava-flooded embayments at the edge of mascon basins. If the heat flow is influenced by structural or compositional anomalies unique to this type of region, the anomalies would affect both measurements. To that extent, they would not be representative of global flux from the Moon. However, the

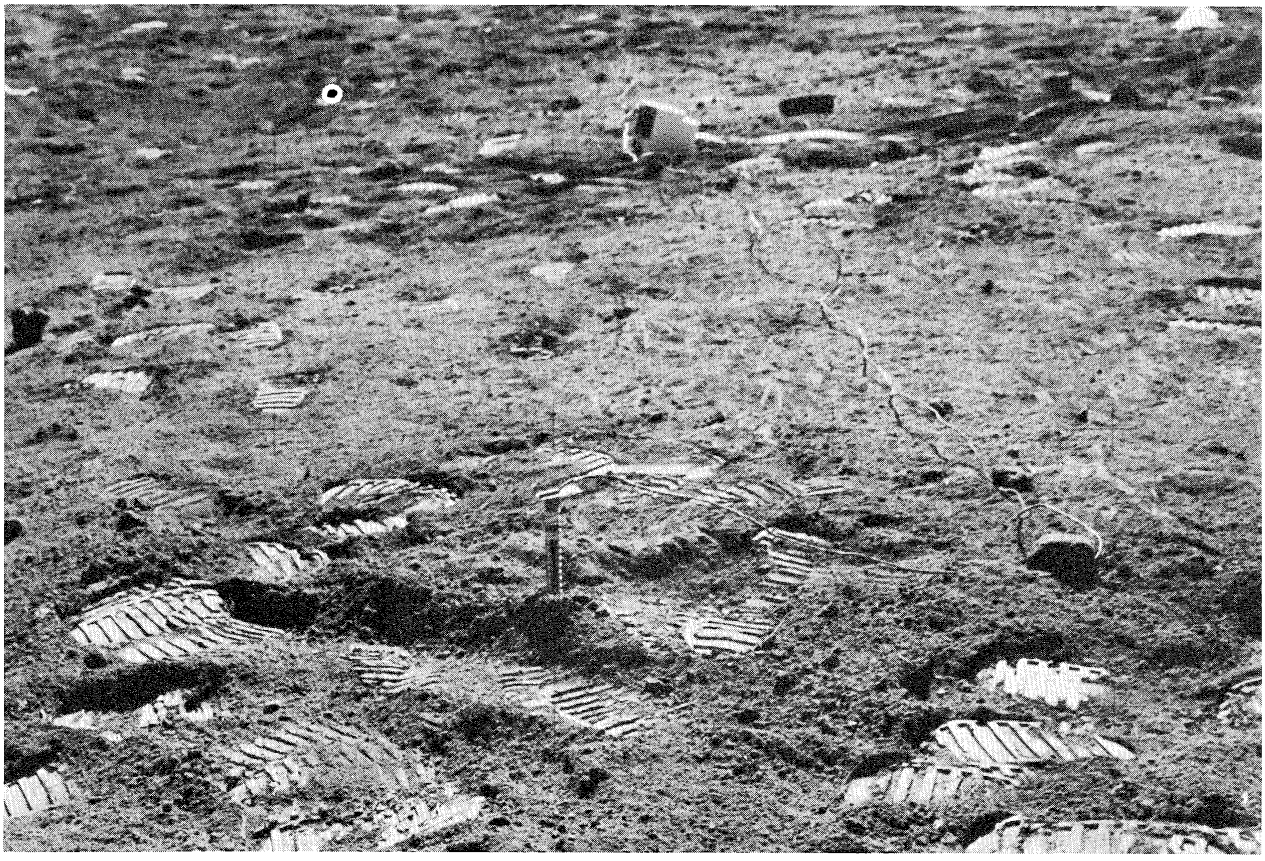

FIG. 9-8.–Photograph of probe 2 borestem protruding from the lunar surface. The heat flow experiment housing is in the background. The thermocouple is in the black portion of cable approximately 10 cm from the top of the stem (AS17-134-20492).

possible compatibility of the results with the microwave emission spectral gradient between 5- and 20-cm wavelengths lends support to the possibility that local anomalies at the two sites are not large.

Despite the reservations in the previous paragraphs, the existing data concerning heat flow from the lunar interior indicate that a significant area of the Moon is characterized by a flux of between 2.5 and 3.0 $\mu W/cm^2$. Numerous thermal history calculations have shown that the contribution of initial heat (e.g., that gained during accretion) to the present surface flux is relatively small (refs. 9-11 and 9-23) even if the Moon were molten throughout initially. Some scientists have suggested that, at the present time, the Moon is thermally at steady state (e.g., ref. 9-24). In either case, it follows that a predominant part of the surface flux (2.0 to 3.0 $\mu W/cm^2$) must result from radioactive isotopes in the Moon. The geochemical data are convincing that most of these isotopes are concentrated in the outer layers of the Moon. In addition, the abundances indicated by the heat flow values would require the heat sources to be located near the surface to prevent melting in the outer several hundred kilometers.

The radiogenic heat production per cubic centimeter of rock can be expressed in terms of the abundance of uranium, because the ratios of the other important long-lived, heat-generating isotopes (^{40}K and ^{232}Th) to uranium are well established and quite uniform in the lunar samples. The heat production per unit volume at the present time in W/cm^3 is approximately 0.71 times the uranium abundance in parts per million (e.g., refs. 9-23 and 9-25). If most of the uranium is concentrated within 300 km of the surface so that it contributed to the present flux, then the total lunar uranium abundance required to contribute 2.0 to 3.0 $\mu W/cm^2$ to the heat flow is approximately 0.05 to 0.075 ppm. These abundances are much greater than chondrites and significantly higher than estimates of the Earth abundance of approximately 0.03 ppm (ref. 9-4).

SURFACE TEMPERATURES DEDUCED FROM THERMOCOUPLE MEASUREMENTS

At each of the two heat flow holes, one of the thermocouples is embedded in a section of the cable that is approximately 15 cm from the top of the borestem and suspended above the lunar surface as shown in figure 9-8. These thermocouples, in radiative balance with the lunar surface, with the solar flux, and with space, thus provide a measurement of the surface brightness temperature throughout the lunation. The flux balance equation governing the thermocouple temperature is

$$2\pi a_c dl \epsilon_c \sigma T_c^4 = 2\pi a_c dl F_{c\text{-}m} \epsilon_m \alpha_{cir} \sigma T_m^4 + 2 a_c dl S \alpha_{cs} \sqrt{1 - p^2} + 2\pi a_c dl S A \alpha_{cs} F_{c\text{-}m} \cos\lambda \sin\phi \quad (9\text{-}13)$$

where T_c = thermocouple temperature
T_m = lunar surface brightness temperature
a_c = radius of thermocouple cable
dl = elemental length of cable
ϵ_c = infrared emissivity of cable
α_{cir} = infrared absorptivity of cable
α_{cs} = absorptivity of cable to solar flux
$F_{c\text{-}m}$ = view factor of cable to the lunar surface, including the surrounding mountains
p = cosine of the angle between the Sun line and the cable axis, a function of cable orientation and lunar phase angle
λ = selenographic latitude at Taurus-Littrow
ϕ = lunar phase angle measured from local sunrise
ϵ_m = infrared emissivity of the lunar surface ($\cong 1.0$)
S = the mean solar constant of 0.1352 W/cm^2
A = lunar albedo of 0.08
σ = the Stefan-Boltzmann constant

The first term on the right side of equation (9-13) represents flux into the cable element from the lunar surface; the second term represents direct flux from the Sun; the third term represents solar energy reflected diffusely from the lunar surface and impinging on the cable.

The radiative properties of the cable ϵ_c, α_{cir}, and α_{cs} were determined by laboratory measurement before the Apollo 17 mission. The cable orientations for both probe locations were determined from ALSEP photographs.

Solving equation (9-13) for the surface brightness temperature yields

$$T_m = \left[\frac{\epsilon_c \sigma T_c^4 - (S/\pi)\alpha_{cs} \sqrt{1 - p^2} - SAF_{c-m} \cos \lambda \sin \phi}{F_{c-m} \epsilon_m \alpha_{cir} \sigma} \right]^{1/4} \quad (9\text{-}14)$$

During the lunar night, using $\epsilon_m = 1$ and $\epsilon_c = \alpha_{cir}$, equation (9-14) reduces to

$$T_m = \left(\frac{T_c^4}{F_{c-m}} \right)^{1/4} \quad (9\text{-}15)$$

Equations (9-14) and (9-15) assume that the surrounding mountains at Taurus-Littrow are at the same temperature as the surface throughout the lunation. The deviation from this assumption, especially during the lunar day, may be quite large. However, both thermocouples have view factors to the mountains about one-twelfth of the view to the surface. Thus, even large anomalous temperatures on the slopes of surrounding mountains will produce only negligible errors in the surface temperature determination.

Shown in figure 9-9 is a full lunation plot of deduced lunar surface brightness temperatures at Taurus-Littrow. Vertical bars present estimated error bounds. The daytime temperatures were determined solely from the temperature data of the exposed probe 2 thermocouple for two reasons. First, the orientation of the thermocouple at probe 1 was much more difficult to obtain from the photographs. Second, the probe 1 thermocouple appeared to have a more substantial view of the radiation shield atop the borestem; the radiation shield is a highly reflective square of aluminized Mylar that could add a substantial unknown factor to equation (9-14).

The nighttime temperatures are not subject to the errors due to uncertainties of the cable orientations, and the data shown are an average of the two thermocouple reductions. Nighttime surface temperatures deduced from each of the two above-surface thermocouples differed by no more than 2 K throughout the lunar night. The data gaps near sunset and immediately following sunrise correspond to times of rapid temperature changes. During these periods, equation (9-14) loses its validity because the finite time constant of the thermocouple cable must be considered.

From the data of figure 9-9, a mean surface temperature of 215 K (± 5 K) was calculated for the Taurus-Littrow site, indicating a mean temperature rise of approximately 39 K between the surface and the top probe sensors. Only a small part of this mean temperature rise (no more than 5 K) can be accounted for by the measured heat flow. The mean temperature gradient is due mainly to the contribution of radiative heat transfer within the highly porous dust layer approximately 2 to 3 cm thick at the surface. During the warm lunar day, heat is transferred more effectively into the lunar surface than it can be transferred out during the cold lunar night. To conserve net flux over a lunation, a mean temperature gradient is established, mainly confined to the porous surface layer. A similar phenomenon

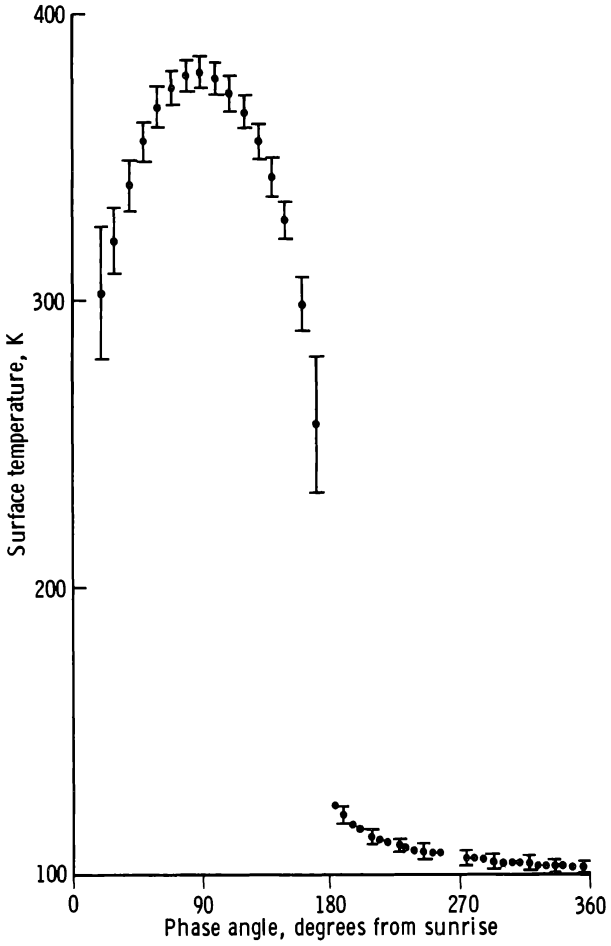

FIGURE 9-9.–Surface temperatures determined from thermocouple measurements. Vertical bars are estimates of the error limits.

was observed at the Apollo 15 site, where a mean temperature rise of 45 K was measured between the surface and the top probe sensor. (The value of 35 K reported in reference 9-11 has been revised to include the effect on the occlusion by local topography of the early morning Sun at Rima Hadley and the refinements in the thermocouple-to-surface temperature-reduction calculation.) The total rise in mean temperature actually takes place almost entirely over the first few centimeters.

The temperature dependence of the diurnal heat transfer in the near-surface layer can be examined quantitatively by postulating an effective thermal conductivity that is a function of temperature.

$$k(T) = k_c + k_r \times T^3 \qquad (9\text{-}16)$$

The functional form of equation (9-16) has been verified experimentally for silicate powders in vacuum (ref. 9-26). Cremers and Birkebak (ref. 9-27) have also found the conductivity of returned lunar fines to fit a functional relationship of the form of equation (9-16). The parameter R_{350}, which equals $k_r(350^3)/k_c$, was first used by Linsky in examining this phenomenon (ref. 9-28) and represents a measure of the radiative contribution to the heat transfer in the upper few centimeters. By using one-dimensional models of the lunar regolith, it is found that R_{350} must be within the range 1.7 to 2.2 for the Apollo 17 site and between 2.5 and 3.0 for the Apollo 15 site to produce the observed mean temperature gradients. The range of values for the Apollo 17 site correspond closely to the value of 1.48 obtained by Cremers and Birkebak for returned Apollo 12 samples (ref. 9-27). Similar measurements on Apollo 11 samples yielded R_{350} values approximately equal to 0.5. It is important to note, however, that even very slight disturbances to the in situ configuration of the porous lunar fines may have large effects on the thermal properties of the fines. In any case, the fact that a large mean temperature gradient has been observed at both lunar heat flow sites, separated by 700 km, strongly indicates that a porous layer in which radiative heat transfer plays a dominant role is a prevalent feature of the lunar surface, at least in the mare regions.

It is fortunate that the more accurate surface temperature determinations are made during the lunar night because the postsunset surface cooldown data are most strongly constrained by the thermal properties within the top 5 to 10 cm of the surface. Figure 9-10 shows, on an expanded scale, the reduced lunar surface nighttime temperatures at the Apollo 15 and Apollo 17 sites. The solid curves represent best-fitting computer models of the thermal properties of the upper 15 cm of regolith at each site. The density and mean conductivity profiles used to produce the theoretical cooldown curves are shown in the inset figure. (Mean conductivity is the effective conductivity at a given depth at the mean temperature of that depth.) The density profile used for the Apollo 15 site is based on inferences drawn from drill

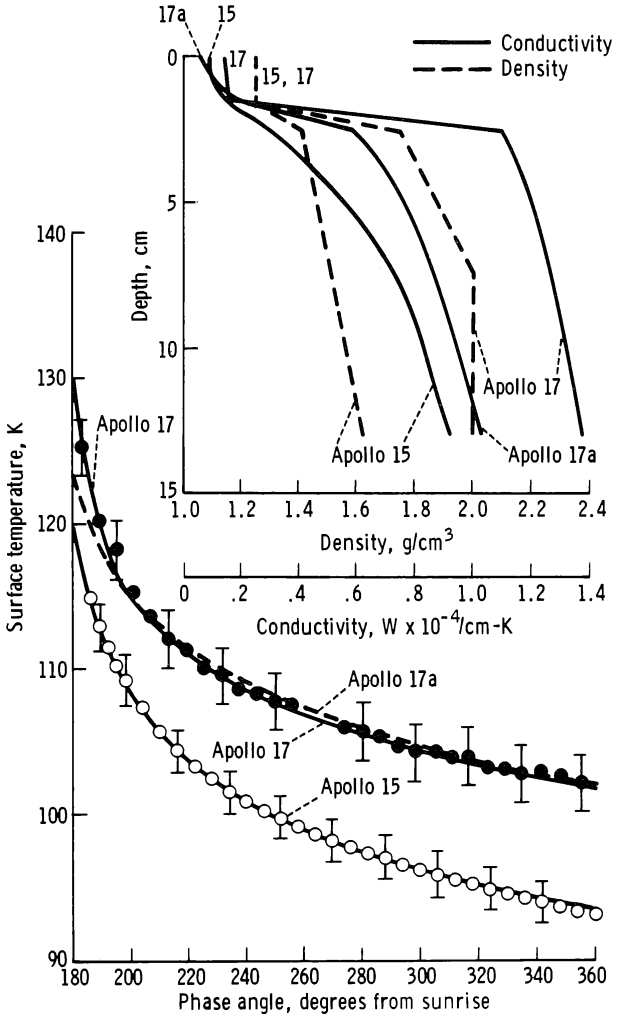

FIGURE 9-10.–Temperatures during the lunar night at the Apollo 17 (solid dots) and Apollo 15 (open circles) sites. Vertical bars are estimated errors. The continuous curves are theoretical curves derived from the thermal property models shown in the inset.

core penetration rates and surface disturbance caused by crew activity reported by J. Mitchell (personal communication, 1972) of the Apollo 15 soil mechanics team. The density profile for the Apollo 17 site was determined from preliminary examination of returned core tube samples (D. Carrier, personal communication, 1973). In both the Apollo 15 and 17 models, the heat capacity as a function of temperature was taken from Robie et al. data (ref. 9-29) on returned Apollo 11 samples. In both models, a low conductivity layer approximately 2 cm thick is required to fit the steep drop in surface temperature immediately after sunset. The Apollo 15 model then requires a steep, but not discontinuous, rise in conductivity with depth down to 5 cm to produce the increased flattening of the cooldown curve through the lunar night. The Apollo 17 model, however, requires a very sharp rise in conductivity at a depth of approximately 2 cm to produce the abrupt flattening of the cooldown curve at a phase angle of approximately 190°. The subsequent increase in conductivity with depth is slight enough so that the Apollo 17 model may be considered essentially a two-layer model. The large jump in conductivity at 2 cm is also supported by the preliminary density profile, which indicates a fairly high density quite close to the surface. The Apollo 15 density profile, however, supports the possibility that a substantial conductivity gradient exists over the upper 30 cm of the regolith.

The most critical surface temperature data required for the purpose of determining thermal regolith profiles are those obtained during the 10 to 30 hr immediately after sunset. Surface temperature data during this period have been the most difficult to obtain from remote infrared brightness scans. The level and steepness of the cooldown data immediately after sunset are controlled almost entirely by the thermal properties of the upper 2 cm. If the very early nighttime data are not sufficiently accurate to constrain the thermal properties of the upper 2 to 3 cm of the dust layer within ± 30 percent, then subsequent attempts to determine deeper conductivity values unambiguously from the flattened part of the cooldown curve will not be possible. For example, the broken-line curve of figure 9-10 fits the nighttime data after 192° phase angle well within the error bands of the data. However, discrepancies in the early postsunset fit produced by different conductivities within the upper 2 cm lead to discrepancies as much as a factor of 2 in conductivity determinations for depths below 2 cm (curve 17a, fig. 9-10 inset).

CONCLUSIONS

During the Apollo missions, two heat flow measurements were successfully made on the lunar surface. Both measurement sites are in similar regional settings in the northeast quadrant of the Moon. The Taurus-Littrow and Rima Hadley sites are located in embayments in the mountainous rims of the Imbrium and Serenitatis mascon basins that have been flooded by mare-type basalts.

Surface brightness temperatures were calculated from the temperature of thermocouples suspended several centimeters above the lunar surface. The mean surface temperature at Rima Hadley throughout a lunation cycle is 207 K. The mean temperature increases with depth very rapidly in the upper few centimeters and is approximately 252 K at a depth of 90 cm. The main reason for this increase of 45 K is the predominant role of radiative heat transfer in the loosely packed upper layer. During the lunar night, the surface temperature at Rima Hadley falls to 93 K. From the cooldown history after sunset, we have deduced that the upper 2 cm of the regolith is characterized by a conductivity of 1.5×10^{-5} W/cm-K. Below this depth, the conductivity increases rapidly and probably in a continuous manner until it reaches values of approximately 1.5×10^{-4} W/cm-K at depths where the probes are emplaced.

At Taurus-Littrow, the mean surface temperature is 216 K and, as in the case of Rima Hadley, increases a few tens of degrees in the upper 2 cm so that, at a depth of 67 cm, a mean temperature of 254 K is measured. The minimum temperature just before lunar dawn is 103 K, 10 K higher than that at Rima Hadley. This higher temperature is primarily attributable to the existence of a relatively high conductivity layer at a depth 2 cm below the surface. From the point of view of thermal properties, the regolith at Taurus-Littrow can be described as two layers: an upper 2-cm, loosely packed layer of very low conductivity (1.5×10^{-5} W/cm-K) in which heat transfer by radiation predominates and a lower layer with much higher conductivity ($> 1.2 \times 10^{-4}$ W/cm-K) and higher density (1.8 to 2.0 g/cm^3).

Subsurface temperature and conductivity measurements at depths below 90 cm, where the large diurnal variations are negligibly small, indicate a steady-state

heat flow through the surface at Rima Hadley of 3.1×10^{-6} W/cm^2 and at Taurus-Littrow of 2.8×10^{-6} W/cm^2 with an estimated error of ± 20 percent. These fluxes are deduced from average temperature gradients in the regolith between 1.3 and 1.7 K/m and an average conductivity in the range of 1.7×10^{-4} to 2.0×10^{-4} W/cm-K. Conductivity generally increases with depth in the regolith although some layering, with high conductivity materials overlying lower conductivity materials, is found at both sites (table 9-VI). A conductivity value of almost 3×10^{-4} W/cm-K was measured at the bottom of probe 1 at the Apollo 17 site. Thermal gradients decrease with depth, in some cases, in response to the increase in conductivity. At Taurus-Littrow probe site 2, a large decrease in gradient with depth is possibly attributable to a large subsurface boulder in close proximity to the probe.

The heat flows at both sites are affected to some extent by local topography. Preliminary estimates indicate that a correction of −15 to −25 percent may be applicable to the Taurus-Littrow values because of the adjacent massifs. However, a more refined analysis is required.

The heat flow measured at the two sites is approximately one-half the average heat flow of the Earth (6.3×10^{-6} W/cm^2). If these two values are representative of heat flow from the Moon as a whole, then a heat flow of one-half that of the Earth requires a heat production per unit mass for the lunar interior of more than twice that of the Earth. This statement assumes both planetary bodies are near steady state so that total surface heat loss is nearly equal to the present interior heat production.

Because the long-lived radioisotopes of ^{40}K, ^{235}U, ^{238}U, and ^{232}Th are the principal source of heat in the Earth and Moon, the heat flow results imply a twofold to threefold enrichment of uranium in the Moon relative to that in the Earth. Lunar samples show that the abundance of potassium relative to uranium is one-third to one-fourth that of the Earth so that, in the Moon, uranium is the main contributor to internal heating. At present, these isotopes must be concentrated in the outer 100 to 200 km of the Moon to avoid extensive melting at shallow depth.

Reinterpretation of Earth-based measurements of microwave brightness temperatures using the new data on regolith thermal and electrical properties will be important in determining the representativeness of the in situ lunar heat flow measurements. Additional, more refined microwave observations of the Moon, especially narrower beamed measurements over discrete portions of the lunar disk, would be valuable in determining possible variations of heat flow over the lunar surface.

ACKNOWLEDGMENTS

The development and testing of instrumentation was performed by Bendix Aerospace Systems Division, assisted in many essential areas by Arthur D. Little, Inc.; Gulfton Industries, Inc.; and the Rosemount Engineering Company. The lunar surface drill was developed by the Martin Marietta Corporation. The authors thank Kenneth Peters of the Lamont-Doherty Geological Observatory for help in much of the numerical analysis. Dr. Robert Jastrow granted generous use of the computer facility at the Goddard Institute for Space Studies. The encouragement and advice of Maurice Ewing of the University of Texas at Galveston, Sidney Clark of Yale University, and Alfred Wechsler of Arthur D. Little, Inc., are gratefully acknowledged.

REFERENCES

9-1. Lee, W. H. K.; and Uyeda, S.: Review of Heat Flow Data. Terrestrial Heat Flow, American Geophysical Union (Washington, D.C.), 1965, pp. 68-190.

9-2. Urey, H. C.: Proc. Natl. Acad. Sci. U.S., vol. 42, 1956, p. 889.

9-3. Gast, P. W.: Limitations on the Composition of the Upper Mantle. J. Geophys. Res., vol. 65, no. 4, Apr. 1960, pp. 1287-1297.

9-4. Wasserburg, G. J.; MacDonald, G. J. F.; Hoyle, F.; and Fowler, W. A.: Relative Contributions of Uranium, Thorium, and Potassium to Heat Production in the Earth. Science, vol. 143, no. 3605, Jan. 31, 1964, pp. 465-467.

9-5. Langseth, M. G., Jr.; and Von Herzen, R. P.: Heat Flow Through the Floor of the World Oceans. The Sea, vol. 4, part I, 1971, pp. 299-352.

9-6. Latham, G. V.; Ewing, M.; Press, R.; Sutton, G.; et al.: Passive Seismic Experiment. Sec. 9 of the Apollo 16 Preliminary Science Report. NASA SP-315, 1972.

9-7. Baldwin, J. E.: Thermal Radiation from the Moon and the Heat Flow Through the Lunar Surface. Monthly Notices, Roy. Astron. Soc., vol. 122, 1961, pp. 513-522.

9-8. Krotikov, V. D.; and Troitskii, V. S.: Detecting Heat Flow from the Interior of the Moon. Soviet Astron., vol. 7, no. 6, May/June 1964, pp. 822-826.

9-9. Tikhonova, T. V.; and Troitskii, V. S.: Effect of Heat from Within the Moon on Its Radio Emission for the Case of Lunar Properties Which Vary with Depth. Soviet Astron., vol. 13, no. 1, July/Aug. 1969, pp. 120-128.

9-10. Smith, B. D.: The Lunar Heat Flow Experiment. Bendix Tech. J., vol. 4, no. 2, 1971, pp. 64-79.

9-11. Langseth, M. G., Jr.; Clark, S. P., Jr.; Chute, J. L., Jr.; Keihm, S. J.; and Wechsler, A. E.: Heat-Flow Experiment. Sec. 11 of the Apollo 15 Preliminary Science Report. NASA SP-289, 1972.

9-12. Langseth, M. G., Jr.; Drake, E. M.; Nathanson, D.; and Fountain, J. A.: Development of an In Situ Thermal Conductivity Measurement for the Lunar Heat Flow Experiment. Thermal Characteristics of the Moon. AIAA Progress in Astronautics and Aeronautics Series, vol. 28, MIT Press (Cambridge, Mass.), 1972, pp. 169-204.

9-13. Jaeger, J. C.: Conduction of Heat in an Infinite Region Bounded Internally by a Circular Cylinder of a Perfect Conductor. Australian J. Phys., vol. 9, no. 2, June 1956, pp. 167-179.

9-14. Keihm, S. J.; Chute, J. L.; Peters, K.; and Langseth, M. G., Jr.: Apollo 15 Measurement of Lunar Surface Brightness Temperatures: Thermal Conductivity of the Upper 1-1/2 Meters of Regolith. Earth Planet. Sci. Letters, vol. 19, no. 3, July 1973.

9-15. Horai, K.; Simmons, G.; Kanamori, H.; and Wones, D.: Thermal Diffusivity and Conductivity of Lunar Material. Science, vol. 167, no. 3918, Jan. 30, 1970, pp. 730-731.

9-16. Buhl, D.; Welch, W. J.; and Rea, D. G.: Anomalous Cooling of a Cratered Lunar Surface. J. Geophys. Res., vol. 73, no. 24, Dec. 15, 1968, pp. 7593-7608.

9-17. Lachenbruch, A. H.: Rapid Estimation of the Topographic Disturbance to Superficial Thermal Gradients. Rev. Geophys., vol. 6, no. 3, Aug. 1968, pp. 365-400.

9-18. Metzger, A. E.; Trombka, J. I.; Peterson, L. E.; Reedy, R. C.; and Arnold, J. R.: Lunar Surface Radioactivity: Preliminary Results of the Apollo 15 and Apollo 16 Gamma-Ray Spectrometer Experiments. Science, vol. 179, no. 4075, Feb. 23, 1973, pp. 800-803.

9-19. Weaver, H.: The Interpretation of Thermal Emissivity from the Moon. Solar System Radio Astronomy, Plenum Press, (New York) 1965, pp. 295-354.

9-20. Gold, T.; O'Leary, B. T.; and Campbell, M.: Some Physical Properties of Apollo 12 Lunar Samples. Proceedings of the Second Lunar Science Conference, vol. 3, MIT Press (Cambridge, Mass.), 1971, pp. 2173-2184.

9-21. Katsube, T. J.; and Collett, L. S.: Electrical Properties of Apollo 11 and Apollo 12 Lunar Samples. Proceedings of the Second Lunar Science Conference, vol. 3, MIT Press (Cambridge, Mass.), 1971, pp. 2367-2379.

9-22. Strangway, D. W.; Chapman, W. B.; Olhoeft, G. R.; and Carnes, J.: Electrical Properties of Lunar Soil Dependence on Frequency, Temperature, and Moisture. Earth Planet. Sci. Letters, vol. 16, no. 2, Oct. 1972, pp. 275-281.

9-23. Hanks, T. C.; and Anderson, D. L.: Origin, Evolution, and Present Thermal State of the Moon. Phys. Earth Planet. Interiors, vol. 5, no. 5, Oct. 1972, pp. 409-425.

9-24. Turcotte, D. L.; Hsui, A. T.; Torrance, K. E.; and Oxburgh, E. R.: Thermal Structure of the Moon. J. Geophys. Res., vol. 77, no. 35, Dec. 10, 1972, pp. 6931-6939.

9-25. Hays, J. F.: Radioactive Heat Sources in the Lunar Interior. Phys. Earth Planet. Interiors, vol. 5, no. 1, Jan. 1972, pp. 77-84.

9-26. Watson, K. I.: Thermal Conductivity Measurements of Selected Silicate Powders in Vacuum from 150-350 K, II. An Interpretation of the Moon's Eclipse and Lunation Cooling Curve as Observed Through the Earth's Atmosphere from 8-14 Microns. Ph.D. Dissertation, California Institute of Technology, 1964.

9-27. Cremers, C. J.; and Birkebak, R. C.: Thermal Conductivity of Fines from Apollo 12. Proceedings of the Second Lunar Science Conference, vol. 3, MIT Press (Cambridge, Mass.), 1971, pp. 2311-2315.

9-28. Linsky, J. L.: Models of the Lunar Surface Including Temperature-Dependent Thermal Properties. Icarus, vol. 5, no. 6, Nov. 1966, pp. 606-634.

9-29. Robie, R. A.; Hemingway, B. S.; and Wilson, W. H.: Specific Heats of Lunar Surface Materials from 90 to 350 Degrees Kelvin. Science, vol. 167, no. 3918, Jan. 30, 1970, pp. 749-750.